DOI: 10.13009/EUCASS2019-465

DOI: ADD DOINUMBER HERE

ACTiVE – Experimental set up and first results of cold gas measurements for linear aerospike nozzles with secondary fluid injection for thrust vectoring

Sieder-Katzmann, Jan[⋆†]*, Propst, Martin*[⋆]*, Stark, Ralf*[‡]*, Schneider, Dirk*[‡]*,*
General, Stephan[‡], Tajmar, Martin[⋆] and Bach, Christian[⋆]
[⋆]*Technische Universität Dresden*
Marschnerstrasse 32, 01307 Dresden, Germany
[‡]*Deutsches Zentrum für Luft- und Raumfahrt Lampoldshausen*
Im Langen Grund, 74239 Hardthausen, Germany
jan.sieder-katzmann@tu-dresden.de · martin.propst@tu-dresden.de
[†]Corresponding author

Abstract

In cooperation with the DLR Institute of Space Propulsion Lampoldshausen, a cold flow linear aerospike nozzle with four different plugs utilizing thrust vector control through secondary fluid injection has been developed for testing at P6.2.The two main goals of this measurement set up were demonstrated in a pre-test: surface pressure measurements and flow phenomena visualization.During a test run with the reference plug (without secondary injection), the principle working function was verified and critical issues identified.The causes of these problems are analyzed, solutions discussed and implemented.This lays the foundation for a successful subsequent measurement campaign.

1. Introduction

Aerospike nozzles are well known for their height adaptive capabilities and their additional performance potential compared to classical bell nozzles.[1–12] Engines with aerospike nozzles have been in discussion for the replacement of the F-1 engine in the Saturn V rocket (J-2T-250K) and for application in the Space Shuttle Main Engine as well as the Shuttle's successor in the Venture Star project (XRS-2200).[13] Due to manufacturing problems of the composite propellant tanks, the work on the XRS-2200 has been terminated in spite of it's highly advanced development.[14] Besides university projects, like the California Launch Vehicle Education Initiative (CALVEIN),[9] the Dryden Aerospike Rocket Test[15] and Daedalus Astronautics,[16] the aerospike engine came back into focus of research and development with the emergence of new private launch providers. With ARCA Space Coporation,[17] Firelfy Alpha[18] (at the beginning), RocketStar Space,[19] Ripple Aerospace[20] and Pangea Aerospace[21] , several newcomers announced to use an aerospike engine due to the expected performance advantage. The most promising technological approach of thrust vector control (TVC) for engines with low and medium thrust seems to be secondary injection thrust vector control (SITVC).[22] This method prevents the necessity of throttling capability of the engine and the installation of a heavy gimballing system.
To our knowledge, SITVC on aerospike engines has been subject to research and development by mainly two actors: Rocketdyne in the 1960s (report by Silver[23]) and Eilers et al[24–26] at Utah State University around 2010. The report by Silver comprised 33 hot-fire tests on an annular nozzle with a variety of injection positions, secondary mass flows and injection patterns, studying the effect on thrust vectoring performance. Within the MUPHyN-project, Eilers et al. investigated SITVC by combining CFD simulations, cold-flow and hot-fire tests. For three different injection positions, they evaluated the performance of side-force generation in terms of specific impulse for the respective secondary mass flow. They focussed on annular nozzle development with the aim of rather making the system ready to be used in a satellite than obtaining fundamental research data. Both developments neither focussed on linear nozzles nor a specific measurement of the pressure distribution.

Within the frame of the research project ACTiVE at TU Dresden, we investigate secondary injection thrust-vector-control (SITVC) on linear and annular aerospike nozzles, utilizing numerical analyzes and experiments. First simula-

DOI: 10.13009/EUCASS2019-465

tions[27,28] ,accompanied by shallow water experiments,[29,30] have shown the general functionality of this TVC method and laid the foundation for this project. In parallel, a profound literature review[22] revealed that SITVC is a favorable solution to steer rockets and space crafts with aerospike nozzles in general and in case of single chamber engines in particular. However, the accessible data base and technological knowledge on secondary injection for aerospike nozzles is insufficient for an expedient engine development. It is the aim of this project to improve this insufficient data situation.
In cooperation with the Flows Group of the Space Propulsion Institute in Lampoldshausen (German Aerospace Center, DLR), a test campaign was planned to investigate the flow phenomena and the pressure distribution on linear aerospike nozzles with SITVC. For this campaign, an aerospike nozzle test specimen with exchangeable plugs (central nozzle body) is manufactured to meet the specifications of the cold flow test stand P6.2 in Lampoldshausen. Three plugs differ in their geometry in terms of truncation and secondary injection location. A fourth plug without the injection is used as reference. The geometry of the plugs is building on each other with only one modification each. Therefore, the influence of the secondary injection, its location and the truncation of the plug can be evaluated separately. In order to prepare the test campaign conducted in May and June 2019, a pre-test campaign has been conducted in December 2018. The latter had the aim to verify the test specimen design and to identify problems, which could jeopardize the measurements and flow visualization.

The general description of the experimental set up is given in section 2. The focus lies on the used test bench P6.2 at the Space Propulsion Institute and the sensor equipment for surface pressure measurements augmented by the visualization techniques Z-Schlieren and Background Oriented Schlieren (BOS). The test specimen is presented in section 3. Besides the derivation of the contour design and the pressure measurement positions, the variability through exchangeable plugs with different truncation lengths and positions for the secondary injection (SI) are outlined. The results of the pre-test campaign from December 2018 are shown in section 4 and discussed subsequently in section 5.

2. Experimental set up

The cold flow test facility P6.2 has been implemented at the Space Propulsion Institute in late 1998. It is used for nozzle or diffuser tests at ambient and high altitude conditions using gaseous nitrogen (GN2) to avoid humidity condensation within the fluid flow. The test facility provides three gas feeding lines, which can be controlled in pressure and mass flow separately. One feeding line is used in the presented configuration with the reference nozzle expanding into ambient pressure. A second line will be used during the test campaign to feed the secondary injection. A summary of the relevant performance data can be found in table 1.[31–33]

Table 1: P6.2 Performance data[31–33]

System	Data
Gas supply system	
	GN2 cold gas
	Mass flow $\dot{m} \leq 4.2\,\mathrm{kg/s}$
	Regulated total pressure $p_0 \leq 6.0\,\mathrm{MPa}$
	Gas supply: ≈ 989 standard m^3
	Test time $> 120\,\mathrm{s}$ with full flow
Measurement and control system	
	Low frequency (LF) data akquisition system[a]
	Provides up to 64 channels at 1 kHz
	50x Anti-aliasing filter for LF
	Data capacity per test up to 4 GB

[a] 8-16 high frequency channels (up to 100 kHz) available

The mounting interface for the test specimen is located on a frame, as shown in figure 1. A corrugated metal hose with an inner diameter of 125 mm provides the feeding gas and is connected to a diffuser, followed by a flow straightener and a pressure measurement flange used to obtain the total pressure p_0. The last flow component upstream of the test specimen is the Börger-contraction[34–37] , which compresses the flow uniformly into a square 45 mm × 45 mm cross section.
A second interface is defined for the pressure measurement. Sensor blocks, which hold the Kulite® pressure transducers (type XT-154-190M) with corresponding pressure ranges (0.1 MPa, 0.75 MPa, 3.5 MPa), are mounted near the test specimen. Steel tubulations from Scanivalve® are glued into these sensor blocks and are connected to 19-port circular

DOI: 10.13009/EUCASS2019-465

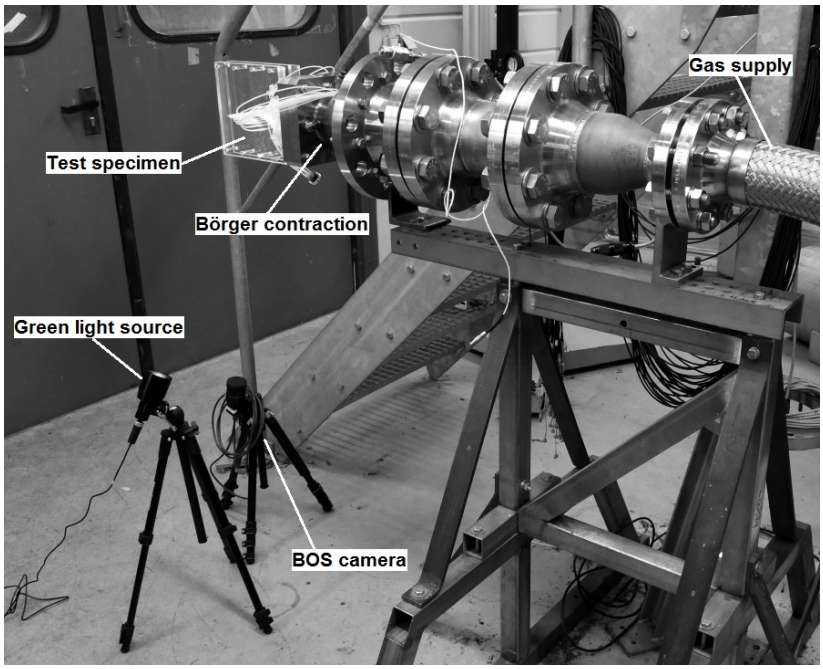

Figure 1: Mounted test specimen and gas supply

pneumatic connectors via Teflon tubes with a diameter of 1.6 mm[1]. The pneumatic connectors are used to enable a faster exchange of the test specimen.

Besides the surface pressure measurements, flow visualization is a key aspect of these pre-tests and the following test campaign. Two different flow visualization systems are used in this set up. A Z-Schlieren set-up, using a Photron® FASTCAM 1024 PCI high speed camera, depicts the flow perpendicular to the two-dimensional nozzle plane (see fig. 2). And a BOS-system depicts the flow lateral from within this plane (see fig. 1). The latter consists of a monochromatic Blackfly S Mono 5.0 MP USB3 Vision camera with a green band filter (MIDOPT FIL BP525/37.5 525 nm) and a green light spot for the most homogeneous illumination possible.
The basic working principle of both visualization techniques is the same: Light is deflected due to a refractive index gradient, e.g. caused by a density gradient. In the Z-Schlieren set up, this deflected light is separated from the undisturbed light with a knife-edge, which is placed in the cut-off plane. In consequence, the Schlieren image shows the density gradients in different shades of gray.[31] The Z-Schlieren are used to image the approximately two-dimensional flow and its phenomena, such as oblique shocks, expansion waves, reflaction shocks etc.
Within the BOS-system, the differentiation between the deflected and the undisturbed light is done via image processing. A self-adhesive foil with a semi-random dot pattern is applied to the nozzle surface. The pattern is specifically adapted to the camera, the lens and especially to the test set up in terms of distances and focal lengths. That pattern is processed by the image software BOSVIS, developed by DLR, which correlates the pattern taken with a reference picture with no flow and images with a gas flow. After the correlation, the displacement of each dot is determined in vertical and horizontal direction and displayed e.g. in a color map. The intention for looking laterally from within the nozzle plane into the flow is at one hand the evaluation of the boundary layer effects due to the acrylic plates of the test specimen. They are used to ensure a two-dimensional flow. On the other hand, it seemed reasonable to assume that separation shocks, which occur in flows with secondary injection, can be depicted and measured in terms of their distance to the injection site. With that distance, an additional parameter is obtained to characterize the flow. For more information on BOS-imaging itself, see Propst et al.[30]

3. Test specimen

After the description of the test stand, an overview on the test specimen follows. Starting with the one-dimensional approach for the dimensioning of the aerospike nozzle, its contour is derived subsequently. This description concludes with the presentation of the pressure measurement and secondary injection positions.

[1] sold as 0.063 inch tubes

DOI: 10.13009/EUCASS2019-465

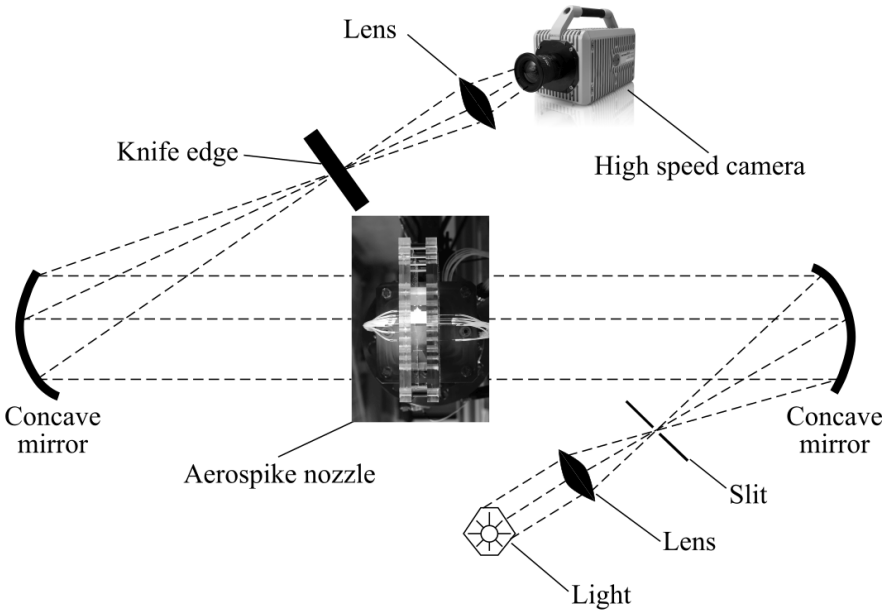

Figure 2: Schematic of the Z-Schlieren set up

3.1 One-dimensional design

The intention for the general design is to fit the test specimen parameters to the test bench capabilities. As shown in table1, the highest realizable mass flow is $\dot{m}_{max} = 4.2\,\mathrm{kg/s}$ and a total pressure of $p_{0,max} = 6\,\mathrm{MPa}$. With the given correlation of mass flow $\dot{m}$ with respect to throat area A_t, total pressure p_0 and the gas properties total temperature T_t, isentropic exponent κ and specific gas constant R:

$$\dot{m} = \frac{p_t A_t \Gamma}{\sqrt{R T_t}} \tag{1}$$

and the auxiliary function for Γ:

$$\Gamma = \sqrt{\kappa \left(\frac{2}{\kappa+1}\right)^{\frac{\kappa+1}{\kappa-1}}} \tag{2}$$

The maximum throat area is derived with $A_{t,max} \leq 300\,\mathrm{mm}^2$ using $p_{0,max}$ and the gas properties for nitrogen at room temperature.

3.2 Nozzle contour

The normalized nozzle contour has been calculated using the FORTRAN program of C. C. Lee[1] adapted for linear aerospike nozzles. Based on the Prandtl-Meyer expansion fan, for each characteristic (straight Mach line) the corresponding flow area necessary to obtain a constant mass flow and in consequence the nozzle contour is derived.
In order to run the program, a few input parameters are necessary. Besides the gas properties, the design pressure ratio $NPR_d = (p_0/p_e)$ between total pressure p_0 and nozzle exit pressure p_e must be specified. Since the nozzle will expand into ambient pressure, the nozzle exit pressure is set to this value. Hence, $NPR_{d,max}$ is limited to ≈ 60 considering $p_{0,max}$. Since all flow states from over-expanded, adapted and under-expanded are of interest, a slightly lower design pressure ratio of $NPR_d = 45$ has been chosen.
Furthermore, a trade-off between nozzle width w_n and nozzle radius R_E (technically the nozzle height) has to be conducted carefully. Both have a direct influence on A_t and are therefore limited. If the nozzle width is chosen too small, the wall shear layer caused by the side walls effects the pressure measurements. Otherwise, if w_n is too high and therefore R_E too small, the nozzle becomes to small for mounting. The finalized input parameters for the nozzle dimensioning and key results are displayed in table 2.
Figure 3 shows the finalized nozzle contour including the truncations at a length of 34.5 % and 64.5 % and the secondary injection sites at 15 % and 40 % - each of the full isentropic length. The truncation has been chosen such that it

DOI: 10.13009/EUCASS2019-465

represents a rather larger and a rather smaller truncation rate, which can both be manufactured and drilled to take in a pressure steel tubulation. Aiming for a rather downstream injection, the two injection locations were chosen such that they are close to the respective nozzle end.

Table 2: Input values and results from nozzle design program

Parameter	**Value**
Input	
Design pressure ratio NPR_d	45
Isentropic exponent κ	1.4
Nozzle width w_n	20 mm
Nozzle radius R_E	36 mm
Output	
Area ratio $\epsilon = A_e/A_t$	4.82
Throat area A_t	298.7 mm^2
Thrust coefficient c_F	1.475

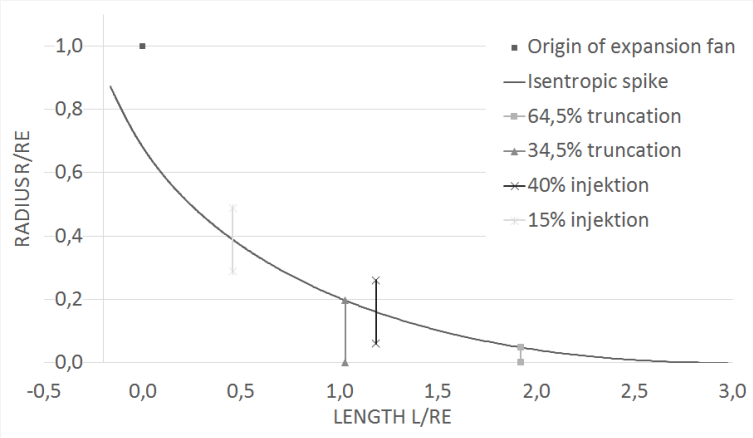

Figure 3: Normalized isentropic nozzle contour with marks for truncations and secondary injection positions

3.3 Realization of the test specimen

The test specimen is designed and manufactured out of several components. It consists of the combustion chamber and four different plugs, each with two acrylic side plates to ensure a two-dimensional flow. All parts are connected by stainless steel screws. A complete test specimen is shown in figure 4.
The combustion chamber is made of stainless steel and its parts are brazed together to ensure leak tightness. Since no real combustion takes places, this component is in one hand the mechanical interface to the test bench with its flange and serves on the other for gas flow distribution. Within the flange, the flow cross section is reduced to a rectangle of 20 mm × 45 mm with a radius on the downstream side. This cross section continues to decrease continuously towards the nozzle throat.
The four different plugs are connected mechanically to the combustion chamber via a t-slot clamp. Each plug is made of aluminum and varies just in one geometric parameter from its predecessor. Plug 1 is called the reference plug with the longer plug length and no secondary injection. The up-following plug 2 has the same length with the downstream secondary injection site. The upstream injection site on a longer plug is called plug 3. Plug 4 shares the injection site with plug 3, but has the higher truncation and is therefore shorter. Each injection is fed by a second gas supply through a steel pipe with 8 mm outer diameter and 1 mm wall thickness.
Two acrylic plates are used to separate the nozzle flow from ambient. Furthermore, in case with secondary injection, the plates separate the two nozzle flows from each other. In order to stiffen the acrylic plates and to ensure a constant spacing between them, eight 8 mm bolts are used with some distance from the nozzle to ensure an unaffected nozzle flow.

DOI: 10.13009/EUCASS2019-465

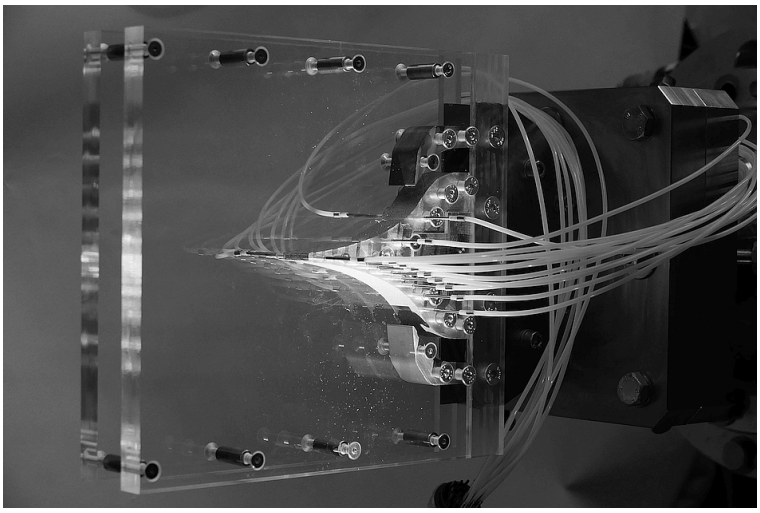

Figure 4: Set up specimen on the test bench

Each plug is equipped with a number of pressure measuring holes, which have all the same center-lined position on each plug. These holes are made with a diameter of 0.5 mm perpendicular to the local surface. On the contour surface with the secondary injection, the measuring holes are spaced with a distance of $\approx$ 7 mm and a doubled density around injection positions. At the same time, the locations of the secondary injection sites coincide with pressure measuring holes of other plugs.
Additionally, in order to ensure comparable pressure measurements between all plugs, two holes are duplicated on the opposite site of the injection, indicated with *u*. In order to evaluate the effects of the wall shear layer development on the pressure measurements, three additional measuring holes are added with 5 mm distance to one wall. They are indicated with *w*.
Each plug is equipped with a measuring hole in the middle of the base and one near the wall. The shorter plug 4 even allowed two additional pressure measuring holes in the center line with a lateral displacement. This enables the analysis, if secondary injection has an influence on the symmetry of pressure distribution of the nozzle base. All pressure measuring locations are summarized in table 3.

4. Results

After describing the test stand and the used specimen, this section points out the obtained results. Starting with the presentation of the operation sequence of the total pressure p_0, the results are displayed with focus on steady state and later on transient effects. The diagrams and pictures display the pressure measurements, the Schlieren and BOS-images and are put into context to each other.

4.1 Test sequence

During the pre-test campaign, conducted on December 14th 2018, one single test run was conducted. Figure 5 shows the commanded test sequence with the control signal *valve opening* and the measured normalized pressure ratio up to $NPR_{p_0} = 25.4$ of the total pressure p_0 with respect to ambient pressure $p_{amb} = 98.7$ kPa. The step signal at the beginning of the sequence was used to 'initialize' the nozzle, in order to remove any residual dust particles especially in the pressure measurement holes. It can be seen, that the total pressure follows the control signal with a delay time of $\approx$ 1 s and reaches its plateau after additional $\approx$ 7 s. Subsequently, the control valve is closed again for 3 s. The following ramp of the control signal over a duration of 25 s opens the control valve fully and holds the plateau for 35 s to ensure sufficient data at a steady state for time averaging.

4.2 Steady state

For the steady state evaluation, the test data obtained in the time window of 1 s and 65 s has been used. Schlieren and BOS images were taken at the first plateau reached within the first 10 s in the sequence due to several reasons described in the discussion (section 5). The presented data contains the measured surface pressure, a lateral cross-plane Schlieren

DOI: 10.13009/EUCASS2019-465

Table 3: Measuring hole locations on the plugs

	Position #	**Axial position [mm]**
Plugs 1-4	01	-4.5
	02 (u, w, uw)	2.5
	03	9.5
	03A	13.0
	04	16.5
	04A	20.0
	05 (u)	23.5
	06	32.3
Plugs 1-3	06A	35.8
	07	39.3
	07A	42.8
	08	46.3
	08A	49.8
	10 (w)	60.3
	Base (w)	69.1
Plug 4	Base (w)	36.9
		(lateral position 0.0)
	Base (o, u)	36.9
		(lateral position ±3)
name affixes:	u: additional hole on opposite side	
	w: additional hole near the wall	
	uw: additional combination of u and w	

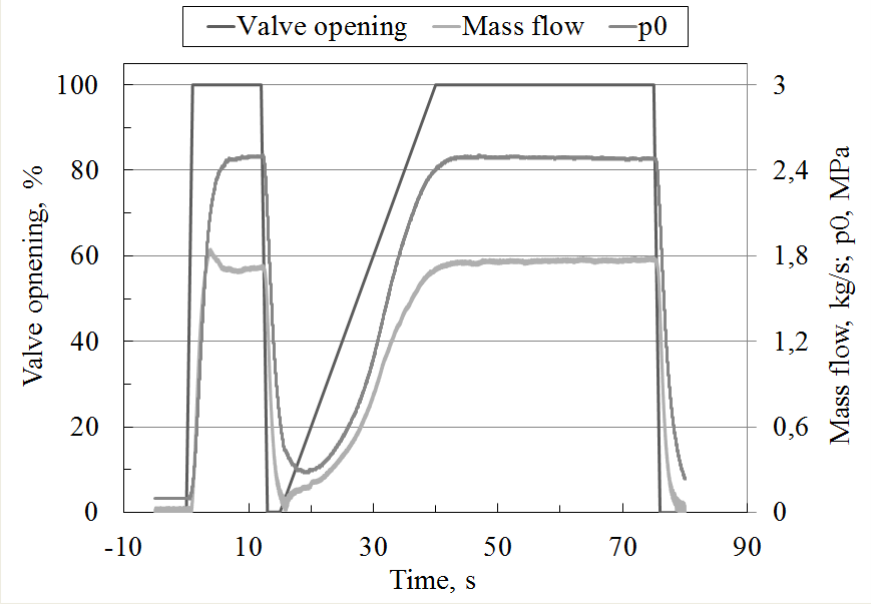

Figure 5: Control sequence, total pressure p_0 and mass flow

image and an in-plane BOS depicting the spike surface on the nozzle side defined by the secondary injection site on the respective plugs.

Figure 6 shows the averaged wall pressure p_w readings over the nozzle surface, normalized with $p_0 = 2.49\,\text{MPa}$. The measurement positions are indicated by their axial as well as their lateral position along the center line of the nozzle or close to the wall. It is also distinguished between the measurement positions on the common and the opposing side with respect to the secondary injection site.

DOI: 10.13009/EUCASS2019-465

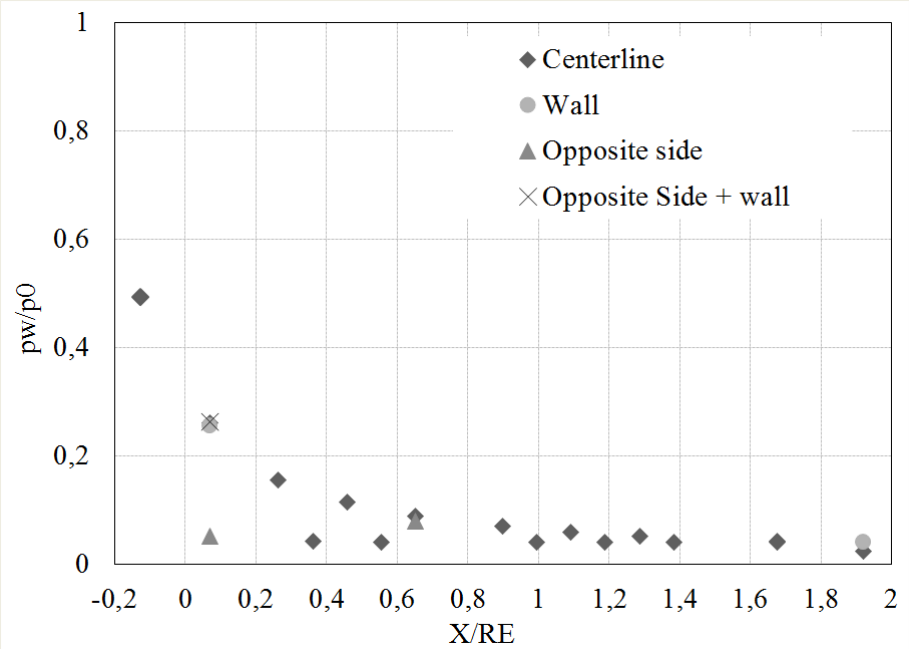

Figure 6: Normalized pressure measurement over the spike surface and base at $NPR = 25.2$

Figure 7 shows a stacked Schlieren picture around time stamp 8 s with an $NPR \approx 25$. The clearly identifiable flow features, such as shear layer, re-compression shock, wake etc., are marked. The shear layer separates the supersonic gas flow from the ambient air and is wide and blurred due to the increasing mixing in the direction of flow. From the nozzle throat towards the plug is the recompression shock visible as a straight line. From the plug's surface the shock is reflected and develops downstream towards the shear layer. At the base of the plug is the wake visible, a recirculation zone, which is name giving for the aerospike nozzle.

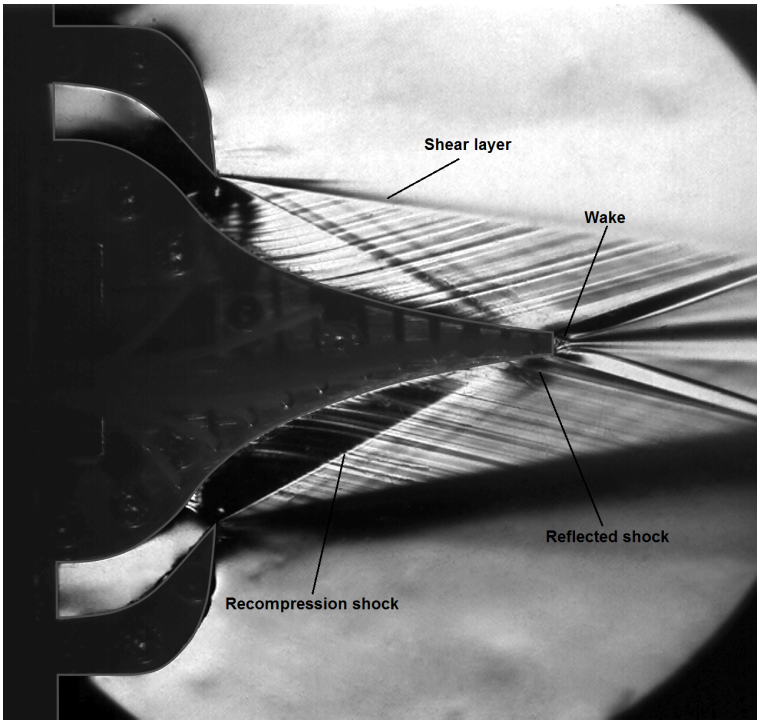

Figure 7: Schlieren picture of the nozzle flow with the shock system at $NPR \approx 25$ (averaged from several single images, scratches and stains retouched)

DOI: 10.13009/EUCASS2019-465

The BOS image taken at 4.980 s is shown in figure 8. Here, the horizontal and the vertical displacement of the image are displayed separately. In this images, no significant shock systems are detectable on the nozzle surface. With the vertical displacement image, a significant growth of the wall boundary layer can be identified. Based on that image, which shows the full width but only a section of the full nozzle length, the boundary layer thickness δ_w at the nozzle end can be estimated to at least 2.5 mm.

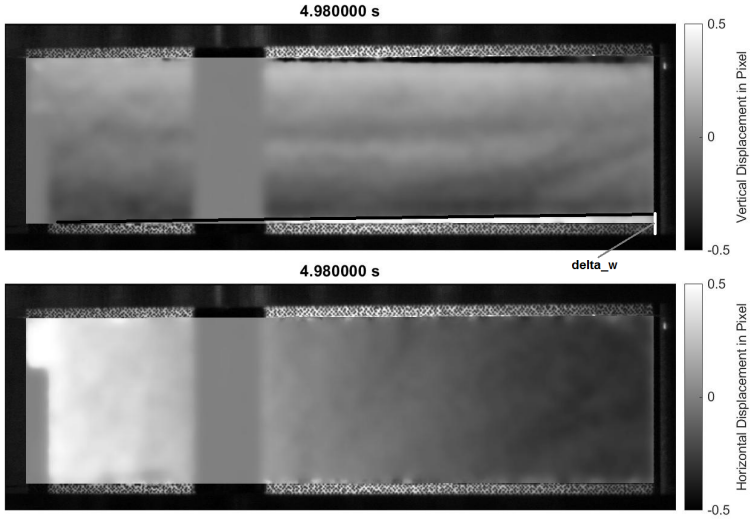

Figure 8: BOS picture (top: vertical displacement, bootom horizontal displacement) of the nozzle flow at $NPR = 24.67$ at time stamp 4.98 s

4.3 Transient behavior

The transient behavior of this linear aerospike nozzle can be observed during the first start up of the test sequence. As it can be seen, the transient process of reaching a stable plateau takes about 5 s, which enables an in-depth analysis of the start-up process. The images of figure 9 show a selection of flow states during the start-up and indicate the recognized flow phenomena. Additionally, shocks visible in the Schlieren image can be correlated with brighter or darker lines in a BOS-image, see fig.10. In this case, the reflection of the reflection shock at the shear layer followed downstream by the first barrel is observed. The corresponding pressure readings from position 02 and 03 (see fig. 11) show that, at the specific time of 1.335 s, the recompression shock has passed the former and is about to reach the latter position.

4.4 Wall effects and nozzle symmetry

Additionally to the center line, measurement ports are included at selected positions, which are located 5 mm towards the wall or on the opposite side of the nozzle. They are used to evaluate the wall effect towards the pressure measurement and the nozzle flow symmetry. Figures 12(a), 12(c) and 12(d) show the transient pressure signal for the respective center line (no index) and the position closer to the wall (index w). It can be seen that for valid pressure measurements (first seconds), the deviation between center line and near wall positions is increasing further downstream. This deviation is much smaller at the nozzle base. The pressure signal intended to show the nozzle flow symmetry is shown in figures 12(a) and 12(b). Index u indicates the measurement signals on the opposing side to the one dedicated to the secondary injection.

5. Discussion

After the presentation of the results, they are evaluated, discussed and put into context. Generally speaking, the test specimen harmonized very well with the test stand in terms of interfaces and flow visualization systems. Nevertheless, it was also possible to identify a number of problem areas for which a solution had to be worked out in preparation for the test campaign in May and June 2019.

DOI: 10.13009/EUCASS2019-465

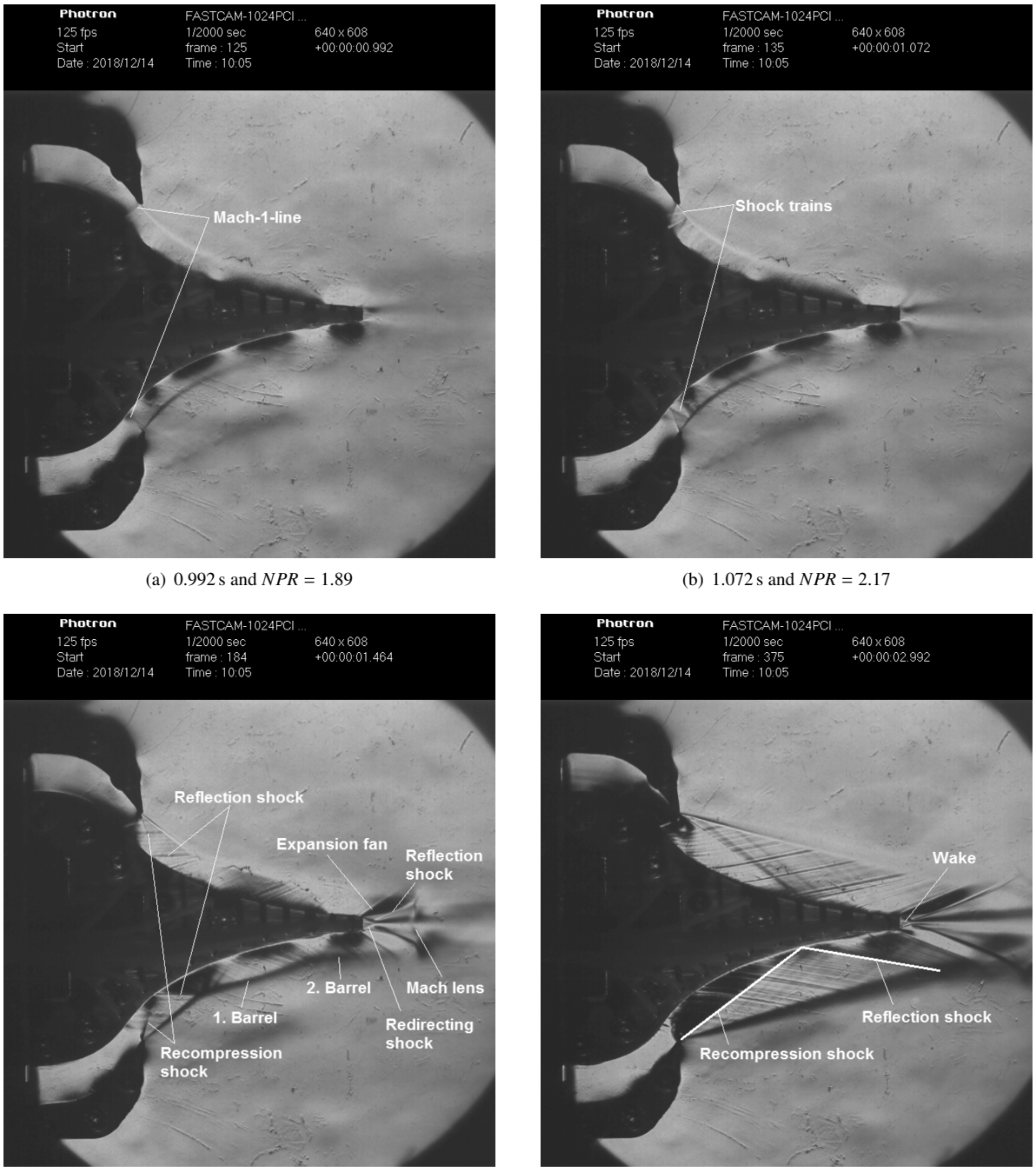

(a) 0.992 s and $NPR = 1.89$

(b) 1.072 s and $NPR = 2.17$

(c) 1.464 s and $NPR = 4.30$

(d) 2.992 s and $NPR = 16.56$

Figure 9: Schlieren images from the start up of the aerospike nozzle flow with identified phenomena

The obtained test data shows that the main flow of the aerospike specimen in combination with the test stand follows the command signal quite agilely. This enables a variation of p_0-plateaus during a single test run in order to obtain sufficient test data for the different flow states (overexpanded, adapted and underexpanded).
Furthermore, the comparison of the calculated (see section 3 equation 1) and the measured mass flow (see fig.5) shows a satisfying agreement with values of 1.71 kg/s and 1.76 kg/s. This difference could have two reasons: The used orifice gauge for the mass flow measurement has not been recalibrated recently, since it is not often used for evaluation. A second source for errors could be the achieved accuracy of the manufactured specimen. Since the equation for the mass flow is proportionally coupled with the realized throat Area A_t, a deviation of the nozzle width w_n can also be a result of the manually applied silicone seal.
The majority of the pressure measurements have worked as expected, especially for the centerline. When compared

DOI: 10.13009/EUCASS2019-465

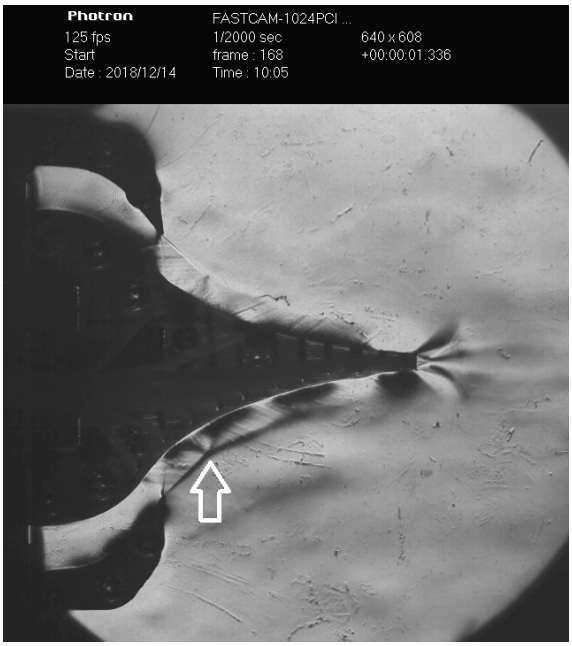

(a) Schlieren image

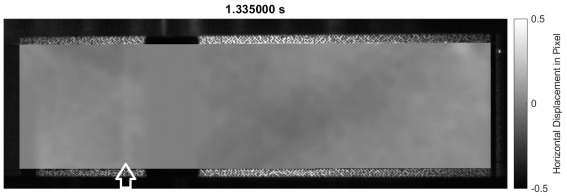

(b) BOS - Horizontal displacement

Figure 10: Traveling shocks during start up of the aerospike nozzle flow at 1.335 s and $NPR = 3.51$

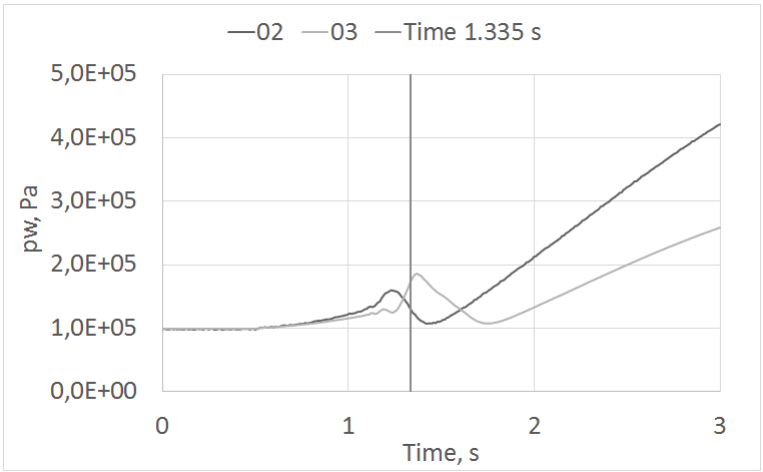

Figure 11: Pressure measurements of position 02 and 03 with time mark at 1.335 s

to a prelimenary numerical calculation (same approach as in Propst et. al.[28]), a good agreement can be found (see fig. 13). However, there were several measurement errors occurring during the run, shown in figures 11-12(d). As for the measurement positions 03A, 04A, 06A, 07A, 08A, 10W and BaseW, the reason for this malfunction can be explained with a not properly fastened pneumatic connector, which lost the leak-tightness after some seconds during the test. Other signals, like position 05U, show some kind of scaling factor error with respect to signal 05. This signal is connected to the well functioning pneumatic connector. Therefore, the reason for the malfunction is different. The

DOI: 10.13009/EUCASS2019-465

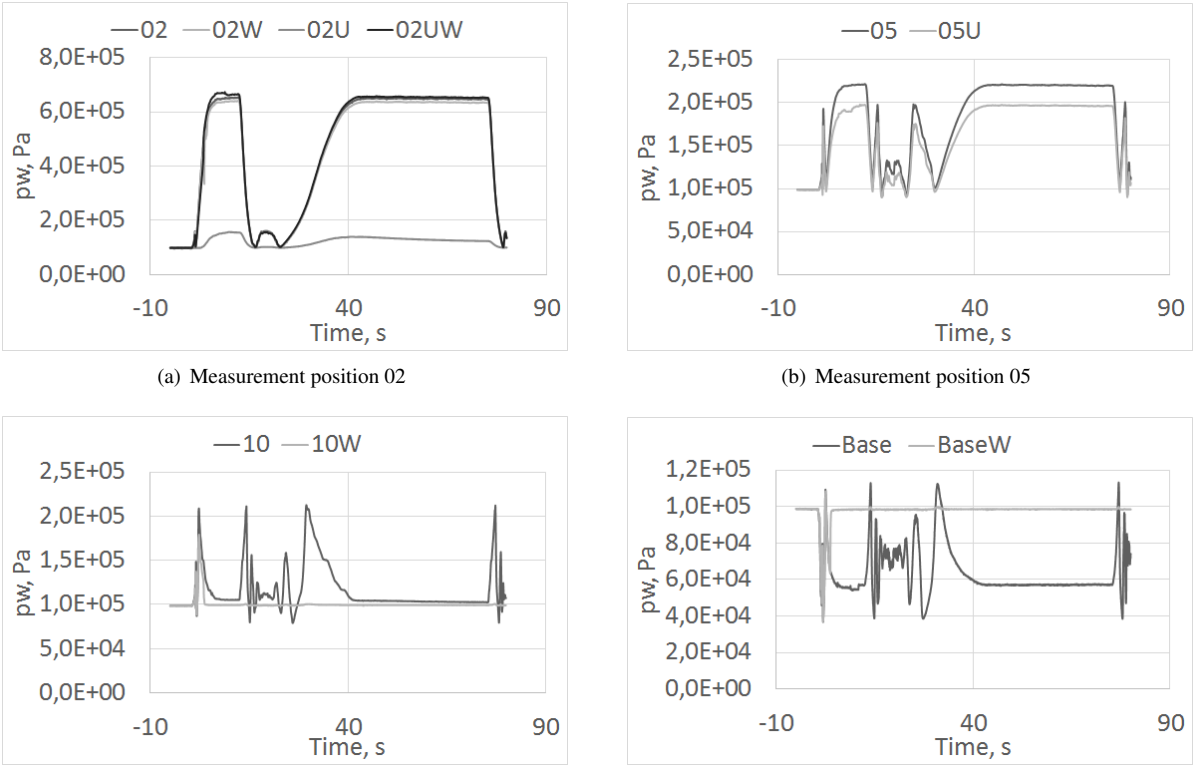

(a) Measurement position 02

(b) Measurement position 05

(c) Measurement position 10

(d) Measurement position Base

Figure 12: Comparison of pressure measurements in the center line, near the wall (index w) and on the opposite side (index u)

most probable explanation is a small leak in between the pressure measurement hole and the sensor. This leak could be a result of an improper glueing of the steel tubulation within the plug, or a damaged Teflon tube. In consequence, the pneumatic connectors will be removed and the Teflon tubes directly connected to the measurement block for the following test campaign. Furthermore, the steel tubulations from the measurement block and their glueing will be renewed.

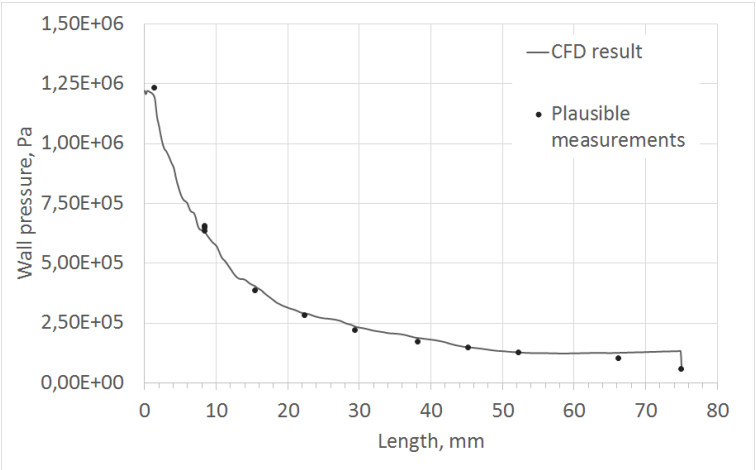

Figure 13: Comparison of plausible pressure measurements from steady state with numerical simulation

The visualization of flow phenomena via Schlieren worked very well and their identification based on literature is easily possible. The BOS images show very promising results with potential for improvement. They enable an evaluation of the wall shear layer development in a two-dimensional specimen (see. fig.8), which can only partially supported by pressure measurements, due to leakages. Especially detachment shocks, which are expected to occur with a secondary

DOI: 10.13009/EUCASS2019-465

injection, seem to be depictable, as the shock reflection can be seen in fig10. In combination, both techniques allow a three-dimensional and transient analysis and measurement of shock systems.

Additonally, there were some technical imperfections in the test specimen, reducing the quality of the flow visualization. The acrylic plates used to ensure a two-dimensional flow were casted. In consequence, their surface was not perfectly even, causing light blurry structures in the Schlieren image. Furthermore, the manufacturing process of drilling and milling caused internal stresses in the material, which are visible in local shading and brightening.
The manually applied silicone seals will be replaced by a laser-cut silicone foil, since the former did not seal the specimen perfectly. Furthermore, the silicone did loosen and smeared the acrylic plates locally (e.g. see fig.9).
After the first flow within the sequence, condensation and icing added disturbances in proper flow visualization with the Schlieren set up. The condensation and icing were caused by very humid weather in combination with the significantly expanded and therefore cooled gas flow, which itself cooled the acrylic plates. When the main flow diminishes, the ambient air reaches the cooled plate and condensates. A proper modification of the sequence will reduce that problem, by starting at a high NPR or p_0 respectively and stepping down, so that the main flow does not interact with the ice and condensate.
A bolt, which was shadowing part of the BOS-image (see fig.8) will be removed in the test campaign. The specimen is stable enough to spare this stiffening. Additionally to the bolt-shadowing, the foil with semi-randomized dot pattern for the BOS visualization peeled off at the beginning of the test sequence. This disrupted the BOS measurements. Caused probably by the low temperatures and high wall shear stresses, the foil disintegrated within the foil plane, so a new method for applying the BOS pattern was searched for. Under-eloxal printing, laser engraving and painting were investigated, none of them seemed to be promising. Therefore, the rather rough structured surface of the plug, made by wire erosion, was tested and showed good results. Hence, the additional pattern application is discarded.

6. Conclusion

A linear aerospike nozzle has been tested at P6.2, verifying the specimen itself, the interfaces and the smooth interaction of the measuring techniques with the nozzle. The two main goals of this joint measurement set-up, to obtain surface pressure measurements and to visualize the flow phenomena, were successfully demonstrated. The results obtained from the imaging methods are very promising with regard to the geometric measurement of the shock systems caused by the secondary injection within the main flow.
For the preparation of the extensive measurement campaign in May/June 2019, this pre-test has also been conducted to identify potential problems. Several sources of leakages were found and approaches to their removal have been discussed and will be implemented. The replacement of the foil with other solutions for applying the dot pattern for the BOS system was inconclusive. However, the granular surface of the wire-eroded plugs provides the necessary surface structure for a successful flow imaging.

In conclusion, the pre-tests conducted in cooperation with the DLR Institute of Space Propulsion in Lampoldshausen are considered to be successful. With the implementation of the knowledge gained from the pre-tests and the derived adjustments, the main measurement campaign promises to produce interesting results.

7. Acknowledgments

We appreciate the assistance and support by: The SAB (Sächsische Aufbaubank - Saxonian Development Bank) and the SMWK (Sächsisches Ministerium für Wissenschaft und Kunst - Saxonian Ministery for Science and Arts), who are funding the project ACTiVE (Ref.-Nr. 100323652); Dietmar Maier, test bench manager of cold gas test bench P6.2 in Lampoldshausen, who did always ensure a smooth test run.

References

[1] C. C. Lee. Technical note - fortran programs for plug nozzle design. Technical report, March 1963.

[2] Gianfranco Angelino. Performance methode for plug nozzle design. *AIAA*, 2(10), 1964.

[3] G. Hagemann, H. Immich, and M. Terhardt. Flow phenomena in advanced rocket nozzles - the plug nozzle. *34th AIAA/ASME/SAE/ASEE Joint Propulsion Conference and Exhibit, Joint Propulsion Conferences*, July 1998.

[4] G. Hagemann, H. Immich, T. V. Nguyen, and G. E. Dumnov. Advanced rocket nozzles. *Journal of Propulsion and Power*, 14(5), September-Oktober 1998.

DOI: 10.13009/EUCASS2019-465

[5] J. J. Korte. Parametric model of an aerospike rocket engine. *AIAA*, (2000-1044), 2000.

[6] A. N. Kraiko and N. I. Tillyayeva. Optimal profiling of the supersonic part of a plug nozzle contour. *Fluid Dynamics*, 35(6):945–955, 2000.

[7] Eric Besnard, Hsun Hu Chen, and Tom Mueller. Design, manufacturing and test of a plug nozzle rocket engine. *AIAA*, (02-4038), 2002.

[8] M. Onofri, F. Nasuti, M. Calabro, G. Hagemann, H. Immich, P. Sacher, and P. Reijasse. Plug nozzles: Summary of flow features and engine performance. *AIAA*, (2002-0584), 2002.

[9] E. Besnard and J. Garvey. Aerospike engine for nanosat and small launch vehicles (nlv/slv). Space 2004 Conference Exhibit, AIAA 2004-6005, September 2004.

[10] M. Nazarinia, A. Naghib-Lahouti, and E. Tolouei. Design and numerical analysis of aerospike nozzles with different plug shapes to compare their performance with a conventional nozzle. volume 11. , AIAC, 2005.

[11] A. Naghib-Lahouti and E. Tolouei. Investigation of the effect of base bleed on thrust performance of a truncated aerospike nozzle in off-design conditions. In *European Conference on Computational Fluid Dynamics*, 2006.

[12] T. Zebbiche and Z. Youbi. Supersonic two-dimensional plug nozzle conception at high temperature. *Emirates Journal for Engineering Research*, 11(2), 2006.

[13] Shannon D. Eilers, Matthew D. Wilson, Dr. Stephan A. Whitmore, and Zachary W. Perterson. Analytical and experimental evaluation of aerodynamic thrust vectoring on an aerospike nozzle. *AIAA*, (2010-6964), Juli 2010.

[14] G. Letchworth. X-33 reusable launch vehicle demonstrator, spaceport and range. Number 0 in AIAA SPACE Forum. American Institute of Aeronautics and Astronautics, January 2019.

[15] T. Bui, J. Murray, C. Rogers, S. Bartel, A. Cesaroni, and M. Dennett. Flight research of an aerospike nozzle using high power solid rockets. In *41st AIAA/ASME/SAE/ASEE Joint Propulsion Conference & Exhibit*. American Institute of Aeronautics and Astronautics (AIAA), 2005.

[16] J. Dennis, S. Shark, F. Hernandez, and J. K. Villarreal. Design of a n2o/htpb hybrid rocket motor utilizing a toroidal aerospike nozzle. In *48th AIAA Aerospace Sciences Meeting Including the New Horizons Forum and Aerospace Exposition*, 2010.

[17] ACRA Space Corporation. Haas 2ca. Online access 15.12.2018.

[18] AviationWeek. Firefly targets late fall for alpha aerospike rocket tests, 2016. Access date 15.12.2018.

[19] RocketStar. Welcome to rocketstar, 2017. Accessed 15.12.2018.

[20] Ripple Aerospace. Oceanic rocketry, 2017. Accessed 15.12.2018.

[21] Pangea Aerospace. Meso rocket, 2018. Accessed 07.07.2019.

[22] C. Bach, S. Schöngarth, B. Bust, M. Propst, J. Sieder-Katzmann, and M. Tajmar. How to steer an aerospike. In *69th International Astronautical Congress*, 2018.

[23] R. Silver. Advanced aerodynamic spike configurations - hot-firing investigations. Final Report AFRPL-TR-67-246-Vol II AD-384 856, Rocketdyne, September 1967.

[24] S. D. Eilers, M. D. Wilson, S. A. Whitmore, and Z. W. Peterson. Side-force amplification on an aerodynamic thrust-vectored aerospike nozzle. *Journal of Propulsion and Power*, 28:811–819, 2012.

[25] S. D. Eilers and S. A. Whitmore. Develompment and testing of a multiple use plug hybrid (for) nanosats (muphyn). In *26th Annual AIAA/USU Conference on Small atellites*, number SSC12-VI-3, 2012.

[26] S. D. Eilers, M. D. Wilson, and S. A. Whitmore. Design of a small scale aerospike nozzle and associated testing infrastructure for experimental evaluation of aerodynamic thrust vectoring. *Utah Space Grant Consortium - Session 2*, May 2010.

[27] M. Propst, J. Sieder, C. Bach, and M. Tajmar. Numerical analysis on an aerodynamically thrust-vectored aerospike nozzle. In *Proceedings of the 63rd German Aerospace Congress (DGLR), Augsburg*, 2014.

DOI: 10.13009/EUCASS2019-465

[28] M. Propst, V. Liebmann, J. Sieder-Katzmann, C. Bach, and M. Tajmar. Maximizing side force generation in aerospike nozzles for attitude and trajectory control. In *69th International Astronautical Congress*, 2018.

[29] J. Sieder, M. Propst, C. Bach, and M. Tajmar. Shallow water experiments to verify a numerical analysis on an aerodynamically thrust-vectored aerospike nozzle. In *Progress in Propulsion Physics – Volume 11*. EDP Sciences, 2019.

[30] M. Propst, L. Rümmler, S. General, V. Liebmann, J. Sieder-Katzmann, C. Bach, and M. Tajmar. Flow visualization and surface measurements of shallow water experiments exemplary for aerospike nozzles with secondary injection. In *Space Propulsion Conference*, 2018.

[31] M. Frey, R. Stark, H. Cieaki, F. Quessard, and W. Kwan. Subscale nozzle testing at the p6.2 test stand. In *36th AIAA/ASME/SAE/ASEE Joint Propulsion Conference and Exhibit*. American Institute of Aeronautics and Astronautics, jul 2000.

[32] H. Kronmüller, K. Schäfer, H. Zimmermann, and R. Stark. Cold gas subscale test facility p6.2 at dlr lampoldshausen. In *6th International Symposium on Propulsion for Space Transportation of the XXI century, Palais des Congress, Versailles, France, 14 - 17 May 2002*, pages 1–8, 2002. LIDO-Berichtsjahr=2002,.

[33] Klaus Schäfer, Christian Böhm, Harald Kronmüller, Ralf Stark, and Herbert Zimmermann. P6.2 cold gas test facility for simulation of flight conditions - current activities. In *EUCASS 2005*, pages 1–7, 2005.

[34] G.-G. Börger. Optimierung von windkanaldüsen für den unterschallbereich, 1973.

[35] G.-G. Börger. The optimization of wind-tunnel contractions for the subsonic range, 1976.

[36] Friedolin Strauss, Chiara Manfletti, Robin Lieberwirth, and Stefan Schlechtriem. Experimental setup on transpiration cooling in supersonic combustion ramjets (scramjets). In *Space Propulsion Conference, Rome, SP2016-3125033*, 2016.

[37] Friedolin T. Strauss, Jan Witte, Matthias Weisswange, Chiara Manfletti, and Stefan Schlechtriem. Experiments on shock-boundary layer interaction and cooling efficiency in a transpiration cooled model scramjet. In *53rd AIAA/SAE/ASEE Joint Propulsion Conference*. American Institute of Aeronautics and Astronautics, jul 2017.